JCTC Journal of Chemical Theory and Computation

pubs.acs.org/JCTC Article

Altered Mechanisms for Acid-Catalyzed RNA Cleavage and Isomerization Reactions Models

Yuqing Xu,* Michael E. Harris, Darrin M. York,* and Kin-Yiu Wong*

Cite This: *J. Chem. Theory Comput.* 2023, 19, 1322−1332 Read Online

ACCESS | Metrics & More | Article Recommendations | Supporting Information

ABSTRACT: RNA strand cleavage by 2′-O-transphosphorylation is catalyzed not only by numerous nucleolytic RNA enzymes (ribozymes) but also by hydroxide or hydronium ions. In experiments, both cleavage of the 5′-linked nucleoside and isomerization between 3′,5′- and 2′,5′-phosphodiesters occur under acidic conditions, while only the cleavage reaction is observed under basic conditions. An *ab initio* path-integral approach for simulating kinetic isotope effects is used to reveal the reaction mechanisms for RNA cleavage and isomerization reactions under acidic conditions. Moreover, the proposed mechanisms can also be combined through the experimental pH-rate profiles.

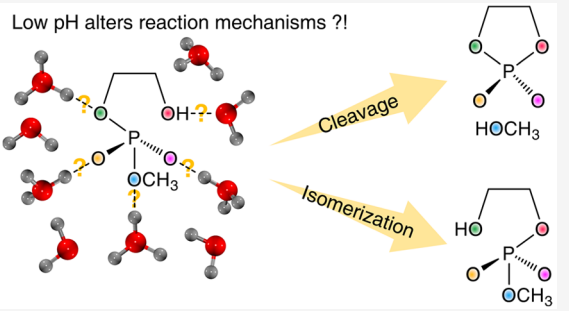

1. INTRODUCTION

The 3′,5′-phosphodiester plays an important role in the chemistry and biochemistry of ribonucleic acid (RNA).[1−9] Its hydrolytic cleavage creates nucleic acid fragments that can be religated by enzymes, together with the sequence-specific catalysis of hydrolysis, which would enable tailoring of the RNA strand in a predesigned manner. Therefore, this reaction has attracted a great deal of interest for decades.

Experimental and theoretical investigations suggested that the cleavage reaction by 2′-O-transphosphorylation proceeds via a pentacoordinated phosphorane intermediate (**2** in Scheme 1) formed by the nucleophilic attack of the $O^{2'}$ on the phosphorus atom in a 3′,5′-phosphodiester (**1a**), and then the $O^{5'}$ leaving group departs and results in a 2′,3′-cyclic monophosphate (**3**). During this process, another competing pathway occurs simultaneously with the P−$O^{3'}$ bond cleaving in the phosphorane and forming an unnatural 2′,5′-counterpart (**1b**), i.e., an isomerization reaction.

Scheme 1. Optional Reaction Pathways for a 3′,5′-Phosphodiester

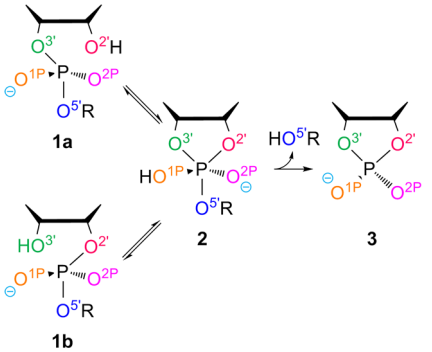

Several model compounds have been used to study the catalytic properties of the 3′,5′-phosphodiester bond.[10,11] For instance, in 1991, Lönnberg measured the kinetics for the cleavage and isomerization of uridylyl(3′,5′)uridine (3′,5′-UpU) in a wide pH range at a temperature of 90 °C.[10] The results showed that under acidic conditions, 3′,5′-UpU could undergo both cleavage and isomerization reactions. However, under basic conditions, only the cleavage reaction was observed (Figure 1). Nevertheless, in spite of decades of research, we still do not fully understand the (altered) mechanisms with pH values, e.g., (i) the differences in the structures of their respective rate-limiting transition states (RLTSs); (ii) the influence of the explicit involvements of hydronium (H_3O^+) ions at low pH; and (iii) the isomerization between the 3′,5′- and 2′,5′-phosphodiesters through a pseudorotation at low pH only. Thus, the underlying motivation of this work is filling the gaps about these mechanisms of the cleavage and isomerization reactions, which is of pivotal significance because actually combinations of these mechanisms can be strategically used by protein and RNA enzyme catalysis.[12−14]

Previously, taking methyl ethylene phosphate as a model for RNA 3′,5′-phosphodiester, using the collaborative synergy between simulations and experiments, the mechanisms of base-

Received: December 16, 2022
Published: February 8, 2023

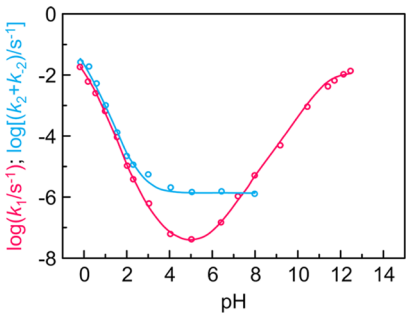

Figure 1. pH-rate profiles at 90 °C for the cleavage of 3′,5′-UpU (red) and the isomerization between 3′,5′- and 2′,5′-UpU (blue). k_1 is the rate constant for the cleavage of 3′,5′-UpU. k_2 is the rate constant for the isomerization from 3′,5′- to 2′,5′-UpU, and k_{-2} is the rate constant for the reverse isomerization. The ratio of k_2/k_{-2} remains 1.0 ± 0.1 over the whole pH range studied.[10] Adapted from ref 5.

and RNase-A-catalyzed 2′-O-transphosphorylation reactions have been successfully unraveled.[12,15−17] In this article, adopting the same model and computational methodology, reaction mechanisms for acid-catalyzed cleavage and isomerization for RNA 3′,5′-phosphodiester bond will be presented. Finally, the two reactions will be combined to reveal the underlying mechanisms in the experimental pH-rate profiles.

2. THEORETICAL BACKGROUND

According to transition state theory, the experimental activation energies $\Delta G^{\ddagger}$ for the RNA cleavage and isomerization in an acidic solution can be evaluated from the reaction rate constant k_{cat}, by using the following expression

$$k_{cat} \approx \frac{k_B T}{h} \exp(-\beta \Delta G^{\ddagger}) \tag{1}$$

where k_B is Boltzmann's constant, T is the absolute temperature, h is Planck's constant, $\beta = 1/(k_B T)$, and the superscript ‡ denotes the transition state. Adopting the latest fundamental physical constants of CODATA 2018,[18] the converted $\Delta G^{\ddagger}$'s are 24.2 kcal mol^{-1} (corresponding to k_{cat} of 2.0×10^{-2} s^{-1}) for the acid-catalyzed cleavage reaction of 3′,5′-UpU and 24.5 kcal mol^{-1} (corresponding to k_{cat} of 1.4×10^{-2} s^{-1}) for the isomerization reaction between 3′,5′- and 2′,5′-UpU, respectively. These values of $\Delta G^{\ddagger}$ can be treated as the estimates of the upper bounds of the experimental activation energies for the acid-catalyzed cleavage of RNA 3′,5′-phosphodiester and the isomerization between RNA 3′,5′- and 2′,5′-phosphodiesters, respectively.

Previous studies on the base- and RNase-A-catalyzed RNA cleavage reaction suggested that the methyl ethylene phosphate should be accurate enough for illustrating the reaction mechanism in an acidic solution.[15−17,19−21] On the basis of the acid dissociation constant (pK_a) values of the nucleophile $O^{2'}$ and a nonbridging phosphoryl oxygen $O^{1P/2P}$, in this study, the reactant is chosen as a neutrally charged solute.

Molecular structures of the reactant state (RS), transition state (TS), intermediate state (IS), and product state (PS) were minimized at the B3LYP/6-31+G(d) level of density-functional theory (DFT)[22,23] with the inclusion of the polarizable continuum model (PCM)[24−28] for implicitly treating the solvent effects (See Table S2 in the Supporting Information for details on comparing this level of DFT with the second-order Møller−Plesset perturbation (MP2) theory.). To ensure the continuity of the PCM potential energy surface (PES), a set of fixed atomic radii was used (See details in the Supporting Information.). Vibrational frequency analyses were carried out to confirm the nature of the minimum and saddle points.[29] The software package GAUSSIAN 09 (Revision C.01) was used for all the electronic-structure and vibrational-frequency calculations.[27]

The measurement of the kinetic isotope effect (KIE) provides one useful means to ascertain details of the nature of the RLTS. The KIE measures the change in the chemical reaction rate constant when an atom(s) in the reactant is(are) substituted by its isotope(s), which is defined as the ratio of the reaction rate constant of the light isotope(s) to that of the heavy isotope(s):

$$\mathrm{KIE} \equiv \frac{\text{Reaction Rate Constant [light isotope(s)]}}{\text{Reaction Rate Constant [heavy isotope(s)]}} = \frac{k_{l_0}}{k_{h_0}} \tag{2}$$

A KIE value that is larger than unity is called a "normal" KIE, because the rate constant of the light isotope is faster than that of the heavy isotope. While an "inverse" KIE means that the KIE value is smaller than unity, i.e., the rate constant of the light isotope is slower than that of the heavy isotope. On account of the sensitivity of KIE values to the molecular structure of an RLTS, measurement of KIE values has been considered as a direct and powerful experimental probe of RLTSs.[19,30−37]

The most widely used formalism to calculate the KIE is the Bigeleisen equation (eq 3),[38−44] in which the Redlich-Teller product rule is satisfied and the KIE is evaluated in terms of harmonic vibrational frequencies only, i.e., in the decoupled rigid-rotor harmonic-oscillator approximation neglecting all quantum tunneling effects

$$\mathrm{KIE}_{\mathrm{BE}} = \left(\frac{\omega_{l_0}^{\ddagger}}{\omega_{h_0}^{\ddagger}}\right)\left[\prod_{i=1}^{3N-7} \frac{\Omega_{l_0,i}^{\ddagger}/\sinh(\beta\hbar\Omega_{l_0,i}^{\ddagger}/2)}{\Omega_{h_0,i}^{\ddagger}/\sinh(\beta\hbar\Omega_{h_0,i}^{\ddagger}/2)}\right]\left[\prod_{i=1}^{3N-6} \frac{\Omega_{h_0,i}^{\mathrm{R}}/\sinh(\beta\hbar\Omega_{h_0,i}^{\mathrm{R}}/2)}{\Omega_{l_0,i}^{\mathrm{R}}/\sinh(\beta\hbar\Omega_{l_0,i}^{\mathrm{R}}/2)}\right] \tag{3}$$

where $\hbar$ is Planck's constant divided by 2π (i.e., the reduced Planck's constant), ω is the imaginary (harmonic) frequency at the transition state, Ω is the real (harmonic) frequency, the superscripts ‡ and R denote the TS and RS, respectively, N is the number of nuclei, and i is the index running over all normal modes.

In order to go beyond the harmonic approximation and to systematically include (nonparabolic) quantum tunneling effects, the Bigeleisen equation is refined in the framework of Feynman's centroid path integral (PI)

$$\mathrm{KIE}_{\mathrm{PI}} = \left(\frac{\omega_{l_0}^{\ddagger}}{\omega_{h_0}^{\ddagger}}\right)\frac{\exp[-\beta(W_{l_0}^{\ddagger} - W_{h_0}^{\ddagger})]}{\exp[-\beta(W_{l_0}^{\mathrm{R}} - W_{h_0}^{\mathrm{R}})]} \tag{4}$$

where W is the centroid effective potential energy calculated at the centroid position of path integrals.[45−47] The mass (isotope) and temperature dependent nature of W distinguishes itself from the (*ab initio*) Born−Oppenheimer potential energy, which is independent of (nuclear) mass and temperature. This refined equation (eq 4) will reduce back to the Bigeleisen equation (eq 3), when the centroid potential is computed in the decoupled rigid-rotor harmonic-oscillator approximation (and neglecting all quantum tunneling effects).

https://doi.org/10.1021/acs.jctc.2c01277
J. Chem. Theory Comput. 2023, 19, 1322−1332

Scheme 2. Reaction Mechanism for the Acid-Catalyzed Cleavage of Methyl Ethylene Phosphate with Explicit H_2O Molecule(s) and H_3O^+ Ion(s) Involved: A Model for RNA Phosphate Transesterification under Acidic Conditions[a]

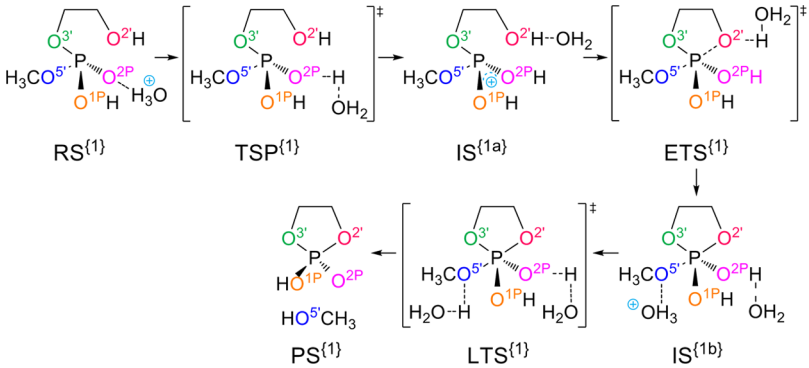

[a]"RS", "TSP", "IS", "ETS", "LTS", and "PS" stand for the reactant state, transition state for the protonation of nonbridging $O^{1P/2P}$, intermediate state, early transition state, late transition state, and product state, respectively.

With the treatment of solvent effects by a dielectric continuum, we used the recently developed automated integration-free path-integral (AIF-PI) method to determine the values of W and then in turn used eq 4 to compute KIE values along the reaction path of the intrinsic reaction coordinate (IRC) on the *ab initio* PES. The AIF-PI method is based on Kleinert's variational perturbation (KVP) theory[46] and makes use of the decoupled instantaneous normal mode coordinate approximation (DINCA) to render the KVP theory applicable to actual molecular systems.[12,15,16,19,47−49] (See details in the Supporting Information.)

In the AIF-PI method, which is implemented in MATHEMATICA,[50] the original solution-phase PES along each normal node is interpolated by a 20th-order polynomial at a step size of 0.1 Å. The centroid potential is computed up to the second order of KVP expansion. Thus, the notation for this level of theory is KVP_2/P_{20}. Through a series of rigorous tests, KVP_2/P_{20} is proved to be a good choice for the AIF-PI method, from which the calculated values of the centroid potential are usually within a few percent from the exact.[47−49]

3. RESULTS AND DISCUSSION

3.1. Acid-Catalyzed Cleavage Reaction. *3.1.1. Reaction Mechanism and Energy Profile.* In order to model the ubiquitous H_3O^+ ions in the acidic solution, we tested a series of different possible pathways (Schemes S1−S7 in the Supporting Information). For the pathways in Schemes S1 and S2, neither the H_2O molecule nor the H_3O^+ ion explicitly participates in the reaction, and intramolecular proton-transfer reactions keep the entire model neutral during the whole reaction. For the pathways in Schemes S3 and S4, proton-transfer reactions are no more intramolecular but by means of two explicit H_2O molecules. Finally, for the pathways in Schemes S5−S7, a number of explicit H_2O molecule(s) and H_3O^+ ion(s) participate in every step of the reaction. In Scheme 2 (i.e., Scheme S5), the nonbridging O^{1P} and O^{2P} get protonated before the nucleophilic attack. We reverse the orders of these two processes in Scheme S6. Scheme S7 illustrates the scenario that these two processes happen concurrently. Since only the model in Scheme 2 returns positive results in terms of both free-energy barriers and KIE values, we will focus on this model in the following discussion. More details for the pathways in Schemes S1−S7 are available in the Supporting Information (some of them probably related to the mechanism(s) around neutral pH values).

The density-functional PCM adiabatic energy profile associated with Scheme 2 is depicted in Figure 2, in which

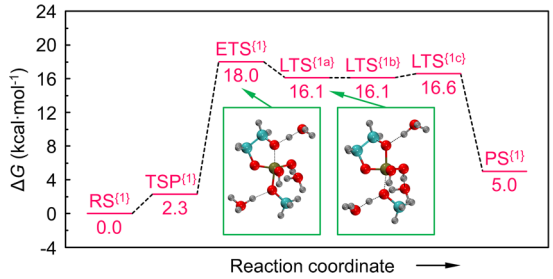

Figure 2. Relative free energies of each stationary point in Scheme 2 along the reaction coordinate. The molecular geometries of the $ETS^{\{1\}}$ and $LTS^{\{1a\}}$ are inserted.

the highest free-energy barrier is 18.0 kcal mol^{-1} (corresponding to the reaction rate constant of 1.1 × 10^2 s^{-1}). Compared with the energy profiles for Schemes S1−S4 that have free-energy barriers at least larger than 30 kcal mol^{-1} (Table S3 in the Supporting Information), this is the only energy profile that has the highest free-energy barrier smaller than the upper bound estimated from the experiment (24.2 kcal mol^{-1}, corresponding to the reaction rate constant of 2.0 × 10^{-2} s^{-1}). Since in the acidic solution the deprotonation of $O^{2'}$−H is not a pre-equilibrium step (in contrast to the base-catalyzed case), then a very critical chemical step to drastically lower the free-energy barrier from ∼30 kcal mol^{-1} to 18.0 kcal mol^{-1} is having both O^{1P} and O^{2P} protonated (Scheme 2). Fortunately enough, the free-energy barrier associated with protonating the second nonbridging $O^{1P/2P}$ is fairly low, which is only 2.3 kcal mol^{-1} ($TSP^{\{1\}}$ in Figure 2).

After both O^{1P} and O^{2P} are protonated, the free-energy barrier associated with the nucleophilic attack (early transition state, ETS) of the $ETS^{\{1\}}$ is monumentally decreased to 18.0 kcal mol^{-1}, where the $O^{5'}$−P bond is slightly lengthened to 1.71 Å and the $O^{2'}$−P bond is not yet formed at 1.82 Å (Table 1), while the deprotonation of $O^{2'}$−H at the $ETS^{\{1\}}$ is basically complete, which is reflected by the 1.27 Å separation. And the distance between $O^{5'}$ and H_3O^+:H is shortened to 1.61 Å, which means a very strong hydrogen bond has already been formed to stabilize the leaving $O^{5'}$ even at the ETS.

https://doi.org/10.1021/acs.jctc.2c01277
J. Chem. Theory Comput. 2023, 19, 1322−1332

Table 1. Interatomic Distances (R) and the Wiberg Bond Order (BO) of Bonds $O^{5'}$−P, $O^{5'}$−H, $O^{2'}$−P, and $O^{2'}$−H for Certain Stationary Points in Scheme 2

	interatomic distance (Å)				bond order			
	$R_{O^{5'}-P}$	$R_{O^{5'}-H}$	$R_{O^{2'}-P}$	$R_{O^{2'}-H}$	$BO_{O^{5'}-P}$	$BO_{O^{5'}-H}$	$BO_{O^{2'}-P}$	$BO_{O^{2'}-H}$
$RS^{\{1\}}$	1.60	2.21	4.39	0.99	0.73	0.02	0.00	0.65
$TSP^{\{1\}}$	1.59	2.36	3.40	0.99	0.77	0.01	0.00	0.64
$ETS^{\{1\}}$	1.71	1.61	1.82	1.27	0.57	0.11	0.45	0.28
$LTS^{\{1a\}}$	1.82	1.22	1.72	1.56	0.45	0.31	0.56	0.13

Table 2. Computed KIE Values of the Transition States for Acid-, Base-, and RNase A-Catalyzed Cleavage Reactions, Respectively, along with the Most Relevant Available Experimental Results for Comparison

	acid (pH = 0)			base (pH = 14)			RNase A (pH = 7)	
	expt	$ETS^{\{1\}}$	$LTS^{\{1a\}}$	expt	ETS	LTS	expt	LTS
$^{18}k_{O^{2'}}$	0.990(4)[a]	0.988	0.988	0.981(3)[b]	1.017[c]	0.967[c]	0.994(2)[d]	0.998[e]
$^{18}k_{O^{5'}}$	1.005(4)[a]	1.013	1.006	1.034(4)[b]	1.006[c]	1.061[c]	1.014(3)[d]	1.026[e]
$^{18}k_{O^{3'}}$		0.998	0.997					
$^{18}k_{O^{1P/2P}}$	0.991(1)[a]	0.994[f]	0.998[f]	0.999(1)[b]	1.004[c]	1.004[c]	1.001(1)[d]	1.006[e]
$^{2}k_{O^{2'}:D}$		4.555	1.632					
$^{2}k_{O^{5'}:D}$		1.414	4.608					
$^{2}k_{D_2O}$		3.686	5.380					
$^{3}k_{O^{2'}:T}$		9.211	1.993					
$^{3}k_{O^{5'}:T}$		1.588	9.590					
$^{3}k_{T_2O}$		6.520	11.887					

[a]Extracted from ref 12, in which the KIEs were measured by competitive methods. [b]Extracted from refs 15 and 56, in which the measured $^{18}k_{O^{2'}}$ value has been corrected for deprotonation. [c]Extracted from ref 16, in which the KIE values were calculated by the same *ab initio* path-integral method at the DFT-B3LYP/6-31+G(d) level of theory. [d]Extracted from ref 12, in which the KIEs were measured by competitive methods. [e]Extracted from ref 12, in which the KIEs were calculated from the Bigeleisen equation. [f]The arithmetic average values of $^{18}k_{O^{1P}}$ and $^{18}k_{O^{2P}}$, *i.e.*, $^{18}k_{O^{1P/2P}} = (^{18}k_{O^{1P}} + {}^{18}k_{O^{2P}})/2$.

Next, a transient intermediate could be formed as a pentavalent phosphorane ($IS^{\{1b\}}$), which is followed by the $LTS^{\{1a\}}$ with the free-energy barrier of 16.1 kcal mol^{-1} (Figure 2). As opposed to the base-catalyzed 2′-O-transphosphorylation reaction, the prior protonations of both O^{1P} and O^{2P} for the acid-catalyzed reaction can also stabilize the formation of this neutral phosphorane intermediate. This stabilization can be reflected by the emergence of the flat $IS^{\{1b\}}$-$LTS^{\{1\}}$ free-energy surface (Figure 2), which we call the $IS^{\{1b\}}$-$LTS^{\{1\}}$ plateau and does not exist in the base-catalyzed case. Similar plateaus were also reported on the hydrolysis of paraoxon by phosphotriesterase and on the methanolysis of cyclic phosphates in the solution.[33,51]

This rather large energy plateau found only in acidic environments would provide many more opportunities for the isomerization between 3′,5′- and 2′,5′-phosphodiesters via a pseudorotation. And it is consistent with the experimental observations that the isomer of 2′,5′-phosphodiester only appears at low pH.[52−55] More importantly, this also suggests that the current model for the RNA cleavage reaction should also be applicable to describing the mechanism of the RNA isomerization and pseudorotation, which will be discussed in the next section.

As shown in Table 1, at the $LTS^{\{1a\}}$, the cleaving $O^{5'}$−P bond is essentially broken at a length of 1.82 Å, while the nucleophilic $O^{2'}$−P bond is basically formed at 1.72 Å. The leaving group $-O^{5'}CH_3$ gets large stabilization by an H_3O^+ ion, which is reflected by the short separation 1.22 Å of $O^{5'}$−H_3O^+:H. And the $O^{2'}$−H bond is now completely cleaved at a distance of 1.56 Å, forming an H_3O^+ ion with a nearby H_2O molecule.

In the $IS^{\{1b\}}$-$LTS^{\{1\}}$ plateau, before forming the final product, there are actually two more TSs ($LTS^{\{1b\}}$ and $LTS^{\{1c\}}$) associated with the complete departure of the protonated leaving group $HO^{5'}CH_3$ and the deprotonation of O^{2P} (Scheme 2). However, both of them do not have KIE values in agreement with experiments (i.e., probably they are not the RLTS). Therefore, in the following discussion we will focus on the $LTS^{\{1a\}}$ in the $IS^{\{1b\}}$-$LTS^{\{1\}}$ plateau. Details for the $LTS^{\{1b\}}$ and $LTS^{\{1c\}}$ are available in the Supporting Information.

3.1.2. Kinetic Isotope Effect Values. In previous studies on base- and RNase-A-catalyzed 2′-O-transphosphorylation reactions, LTSs are the rate-limiting steps, which have higher free-energy barriers than those of ETSs.[12,15−17] While for the acid-catalyzed case, according to the energy profile in Figure 2, the $ETS^{\{1\}}$ is the rate-limiting step. The calculated free-energy barrier associated with the $LTS^{\{1a\}}$ is lower by a mere 1.9 kcal mol^{-1}. In view of the approximation/accuracy of our model, we think that both $ETS^{\{1\}}$ and $LTS^{\{1a\}}$ can be the rate-limiting step in the acidic environment until we make comparisons of their calculated KIE values with experimental ones for the

https://doi.org/10.1021/acs.jctc.2c01277
J. Chem. Theory Comput. 2023, 19, 1322−1332

purpose of rigorous validation of our proposed mechanism (Scheme 2).

As shown in Table 2, surprisingly, the calculated $^{18}k_{O^{2'}}$ (for the nucleophile) at the ETS$^{\{1\}}$ is inverse, which is contrary to the normal value of $^{18}k_{O^{2'}}$ at the ETSs for base- and RNase-A-catalyzed cases. More importantly, this inverse $^{18}k_{O^{2'}}$, together with other KIE values associated with the ETS$^{\{1\}}$, is in excellent agreement with experiments, including the change of $^{18}k_{O^{5'}}$ from large normal (base-catalyzed case) to small normal (acid-catalyzed case) and the change of $^{18}k_{O^{1P/2P}}$ from slightly normal (base-catalyzed case) to slightly inverse (acid-catalyzed case). These encouraging results make the ETS$^{\{1\}}$ qualified for being the rate-limiting step.

We believe this inverse KIE value of $^{18}k_{O^{2'}}$ has roots in the nucleophilic attack of O$^{2'}$ and the deprotonation of O$^{2'}$−H occurring (almost) simultaneously, which make opposite contributions to $^{18}k_{O^{2'}}$. This process is clearly shown in a More O'Ferrall-Jencks diagram (Figure 3). The ETS$^{\{1\}}$ can be

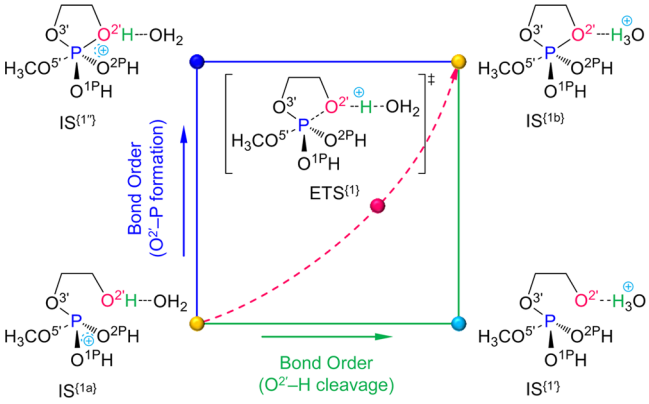

Figure 3. More O'Ferrall-Jencks diagram for the nucleophilic attack of O$^{2'}$ at the P atom. The red solid circle represents the position of the the ETS$^{\{1\}}$ in Scheme 2, which is calculated from the Wiberg bond orders of O$^{2'}$−P and O$^{2'}$−H (values in Table 1). The reaction path connecting the IS$^{\{1a\}}$ (lower-left corner) and the IS$^{\{1b\}}$ (upper-right corner) through the ETS$^{\{1\}}$ is shown. The intermediate states of two extreme scenarios, complete O$^{2'}$−P formation and complete O$^{2'}$−H breakage, are shown in the upper-left and lower-right corners.

thought of as existing on a simplified two-dimensional coordinate, where one axis represents O$^{2'}$−P bond forming and the other represents O$^{2'}$−H bond breaking, respectively. The ETS$^{\{1\}}$ with more O$^{2'}$−H bond cleavage than nucleophilic attack locates in the lower-right quadrant of this plot. Intuitively, two parts of opposite contributions between more O$^{2'}$−H breaking (positive contribution) and O$^{2'}$−P forming (inverse contribution) would offset each other and result in near unity or even a positive KIE value. Therefore, we need to look more deeply into the origin of this inverse KIE value.

In the present AIF-PI method, DINCA is used in the calculation of the centroid potential of path integrals. Conseuently, it allows us to separate the overall quantum effects into contributions from harmonic vibrations, anharmonicity, and quantum tunneling to provide further insight into each KIE value. In this analysis, the total KIE values in eq 4 can be decomposed as follows

$$\mathrm{KIE}_{\mathrm{PI}} = \eta_{\mathrm{har}} h_{\mathrm{anh}} \kappa_{\mathrm{tun}} \tag{5}$$

where η_{har} is the KIE value determined using the Bigeleisen equation (eq 3) with harmonic vibrational frequencies, h_{anh} is the anharmonicity correction factor from all modes with real (positive) frequencies as determined by the KVP$_2$ theory, and κ_{tun} represents tunneling contributions to the computed KIE values corresponding to the imaginary normal modes. The three decomposed factors for $^{18}k_{O^{2'}}$ at the ETS$^{\{1\}}$ are 0.986, 1.002, and 0.999 for η_{har}, h_{anh}, and κ_{tun}, respectively. This indicates that the "harmonic" contribution plays an important role, with both the anharmonic correction and tunneling effect near unity. In fact, η_{har} includes harmonic contribution on the computed vibrational frequencies both at the reactant state and the transition state. Thus, we can define

$$\eta_{\mathrm{har}} = \frac{\eta_{\mathrm{har}}^{\mathrm{TS}}}{\eta_{\mathrm{har}}^{\mathrm{RS}}} \tag{6}$$

where $\eta_{\mathrm{har}}^{\mathrm{RS}}$ and $\eta_{\mathrm{har}}^{\mathrm{TS}}$ specify the isotope effects on harmonicity in the reactant state and the transition state, respectively. In this way, we identify four key normal modes (normal modes #32, #35, #36, and #41 in GAUSSIAN frequency analysis) at the ETS$^{\{1\}}$ that have the largest harmonic contributions, and they are all related to the proton being transferred (Figure 4).

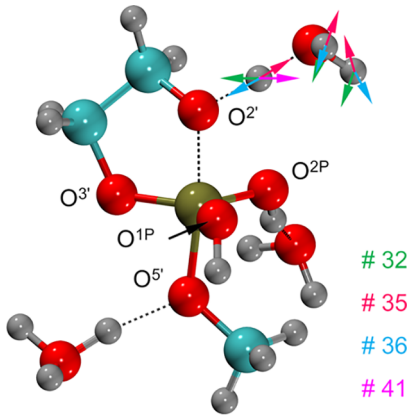

Figure 4. Schematic illustration of the four normal modes identified to have the largest harmonic contributions to the inverse KIE values for $^{18}k_{O^{2'}}$ at the ETS$^{\{1\}}$. All four normal modes are associated with the proton transferred from O$^{2'}$ to a water molecule.

Interestingly, in addition to the ETS$^{\{1\}}$, all KIE values associated with the LTS$^{\{1a\}}$ are also in excellent agreement with experiments (Table 2). This makes the LTS$^{\{1a\}}$ another strong candidate for being the rate-limiting step. Nevertheless, most importantly, since Scheme 2 is so far the only reaction mechanism that has TS(s) in agreement with experimental KIE values and reaction rate constants, then we can conclude that the altered catalytic mechanism for 2′-O-transphosphorylation at pH = 0 has been successfully deduced from the computations and experiments in this work.

Since current experimental KIE values cannot distinguish the ETS$^{\{1\}}$ and LTS$^{\{1a\}}$ definitely, we make many theoretical predictions of KIE values to differentiate between the ETS$^{\{1\}}$ and LTS$^{\{1a\}}$ by future experiments, which are listed in Tables 2, S6, and S7 (Supporting Information). Note here that we try to provide a great amount of theoretical evidence to determine the rate-limiting step, without considering the practical difficulties for these experimental measurements. From Table

https://doi.org/10.1021/acs.jctc.2c01277
J. Chem. Theory Comput. 2023, 19, 1322−1332

Scheme 3. Reaction Mechanism for the Acid-Catalyzed Isomerization of Methyl Ethylene Phosphate with Explicit H_2O Molecule(s) and H_3O^+ Ion(s) Involved: A Model for RNA Isomerization under Acidic Conditions[a]

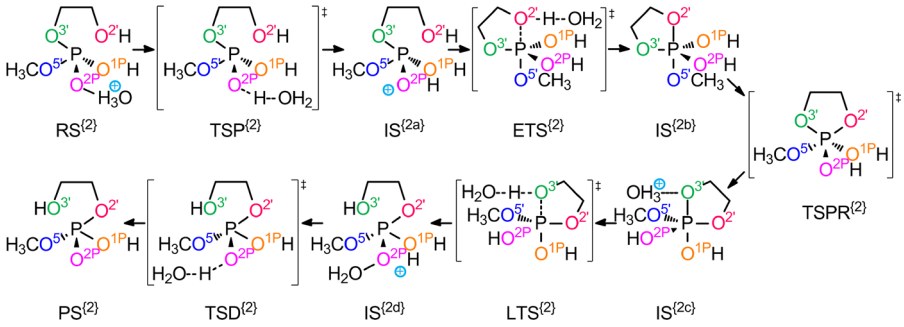

[a]"RS", "TSP", "IS", "ETS", "TSPR", "LTS", "TSD", and "PS" stand for the reactant state, transition state for protonation of the nonbridging $O^{1P/2P}$, intermediate state, early transition state, transition state for pseudorotation, late transition state, transition state for deprotonation of $O^{1P/2P}$–H, and product state, respectively.

2, it shows that not only the single deuterium (D) or tritium (T) substitution for the obvious choices of the two hydrogens, $O^{2'}$:H ($^{2/3}k_{O^{2'}:D/T}$) and $O^{5'}$:H ($^{2/3}k_{O^{5'}:D/T}$), can help us to identify the RLTS but also if the reaction take place in a solution of heavy water (D_2O), particularly in superheavy water (T_2O), the KIE values at the ETS{1} and LTS{1a} are also quite different, e.g., ranging from 3.686 ($^2k_{D_2O}$) at the ETS{1} to 11.887 ($^3k_{T_2O}$) at the LTS{1a}.

3.2. Acid-Catalyzed Isomerization Reaction. *3.2.1. Reaction Mechanism and Energy Profile.* Using the same model compound and computing method as above for 3′,5′-phosphodiester, both stepwise and concerted mechanisms are tested for the acid-catalyzed isomerization between 3′,5′- and 2′,5′-phosphodiesters. For the concerted mechanism, in which the nucleophilic attack of $O^{2'}$ and the departure of $O^{3'}$ occur simultaneously, the estimated free-energy barrier is very high (~40.0 kcal mol^{-1}). Therefore, we focus on the stepwise mechanism, which is also suggested by experimental evidence.[10,57−59]

For the stepwise mechanism, a phosphorane intermediate is formed during the reaction. According to Westheimer's rules, both the nucleophile entry and the leaving group departure must occur at the apical position. Due to the geometric constraint of $O^{2'}$ and $O^{3'}$ lying in one five-member ring in the phosphorane structure, they cannot occupy both apical positions. Therefore, a pseudorotation is needed to transfer $O^{3'}$ to an apical position after the nucleophilic attack of $O^{2'}$ and before the departure of $O^{3'}$.

One of reaction pathways for the isomerization reaction is shown in Scheme 3 (See more details in Scheme S8 in the Supporting Information.). Starting from a neutral reactant RS{2}, first a quick protonation step on the nonbridging O^{1P}/O^{2P} (TSP{2}) occurs to obtain a monocationic 3′,5′-phosphodiester with $O^{2'}$, O^{1P}, and O^{2P} all protonated (IS{2a}). Then the nucleophilic attack occurs, along with $O^{2'}$–H deprotonating to an adjacent water molecule to form a H_3O^+ ion (ETS{2}). With different apical phosphoryl ligands ($-O^{5'}CH_3$, $-O^{1P}H$, and $-O^{2P}H$, respectively) aligning with $O^{2'}$ and phosphorus in the trigonal bipyramidal phosphorane, actually, there are three ETS isomers following the same mechanism (ETS{S8a}−{S8c} in the Supporting Information). After the ETS{2}, a neutral phosphorane IS{2b} is formed. According to experimental pK_a values, this neutral IS adapts to acidic conditions; thus, no proton transfer will take place.[4,60,61] Next, pseudorotation occurs. Overall, the apical position of the phosphorane converts from $O^{2'}$ to $O^{3'}$, and the following rules are restricted for pseudorotation in our simulation:

1) The two oxygen atoms $O^{2'}$ and $O^{3'}$ should take one apical position and one equatorial position. Both apical or both equatorial positions are restrained.
2) One trigonal bipyramidal phosphorane structure contains two apical positions, during the process of pseudorotation, and one apical position exchanges from $O^{2'}$ to $O^{3'}$; the other three ligands all have opportunities to take the opposite apical position.

Therefore, we have a total of six TSs for pseudorotation (TSPR{S8a}−{S8f} in the Supporting Information). For the TSPR{2} in Scheme 3, apical positions convert from $O^{2'}$–P–$O^{5'}$ to $O^{3'}$–P–O^{1P}. After pseudorotation, $O^{3'}$ is transferred to an apical position and ready to depart (LTS) to complete isomerization. Similar to ETSs, LTSs also have three isomerides, with different ligands pairing with $O^{3'}$ taking apical positions. During the departure, one H_3O^+ ion donates one proton to $O^{3'}$ for its negativity. Then the system comes to a cationic 2′,5′-phosphodiester with $O^{3'}$, O^{1P}, and O^{2P} protonated (IS{2d}). According to pK_a values, it needs a deprotonation process of O^{1P}–H/O^{2P}–H (TSD{2}) to get to a neutral product, which can be considered as a reverse process of TSP{2}.

Relative free-energy barriers of each TS in Scheme 3 are shown in Figure 5. In Figure 5, the energy profile shows high symmetry, which is consistent with the symmetric reaction pathway shown in Scheme 3. From an overall perspective, the

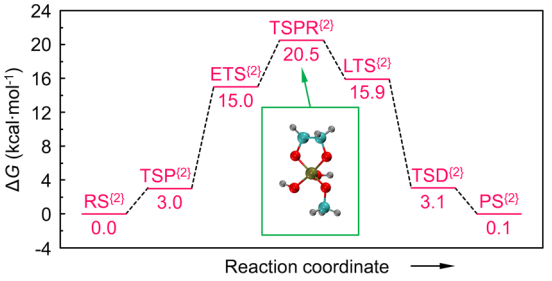

Figure 5. Relative free energies of each stationary point in Scheme 3 along the reaction coordinate. The molecular geometry of the TSPR{2} is inserted.

https://doi.org/10.1021/acs.jctc.2c01277
J. Chem. Theory Comput. 2023, 19, 1322−1332

TSPR$^{\{2\}}$ is the rate-limiting step, with a free-energy barrier $\Delta G^{\ddagger}$ equal to 20.5 kcal mol^{-1} (corresponding to the reaction rate constant of 3.5 s^{-1}). On the other hand, free-energy barriers for the isomer groups of ETSs, TSPRs, and LTSs range from 15.0 to 16.0 kcal mol^{-1}, from 19.4 to 21.1 kcal mol^{-1}, and from 15.1 to 16.1 kcal mol^{-1}, respectively (Table S9 in the Supporting Information). The small discrepancies in the free-energy barriers between each isomer groups suggest that all these reaction pathways through corresponding TSPR isomers have comparable opportunities to take place in practice.

Moreover, looking into the molecular structures of each TSPR isomer can help us to understand the pseudorotation more deeply. The pseudorotation process involves an interconversion of a pentacoordinated trigonal bipyramidal species whereby there is an exchange of two ligands in apical positions with two other ligands in equatorial positions. This process can be visualized as a conformational rearrangement course that involves two concerted bending motions, a contraction of the angle between two apical ligands and a widening of the angle between two equatorial ligands. In other words, after pseudorotation, the bond angle between two apical ligands bends from ∼180° to ∼120°, i.e., from two apical positions to two equatorial positions, while the bond angle between two other ligands expands from ∼120° to ∼180°, i.e., from two equatorial positions to two apical positions. For each TSPR isomer, it is found that accompanied with exchanging apical positions between O$^{2'}$ and O$^{3'}$, TSPRs for exchanging between two −O^{1P}H and −O^{2P}H groups (E.g., the TSPR$^{\{S8c\}}$ exchanges apical positions from O$^{2'}$−P−O^{1P} to O$^{3'}$−P−O^{2P}, and the TSPR$^{\{S8f\}}$ exchanges apical positions from O$^{2'}$−P−O^{2P} to O$^{3'}$−P−O^{1P}.) have slightly lower free-energy barriers (but still is the rate-limiting step along respective reaction coordinates), relative to respective barriers of TSPRs for exchanging between the −O$^{5'}$CH$_3$ group and one −O$^{1P/2P}$H group [E.g., the TSPR$^{\{2\}}$ (i.e., TSPR$^{\{S8a\}}$) exchanges apical positions from O$^{2'}$−P−O$^{5'}$ to O$^{3'}$−P−O^{1P}.]. This phenomenon can be understood by the electronic charge distribution and hyperconjugative interactions between corresponding molecular orbitals (See details in the Supporting Information.).

3.2.2. Kinetic Isotope Effect Values. From the energy profile in the previous subsection, it clearly shows that TSPRs have the highest and consistent free-energy barriers with experimental measurements along each reaction pathway. This conclusion is quite different from previous works on RNA isomerization, which all predict that pseudorotation is unlikely to be the rate-limiting step. To support this statement, we calculate the KIE values for single ^{14}C- or ^{18}O-substitution and list the results in Table 3. Taking into account all of the competitive reaction pathways via each TSPR isomer shown in Scheme S8 (Supporting Information), the computed KIE values are averaged for each TS group, e.g., the TSP group (one isomer), ETS group (three isomers), TSPR group (six isomers), LTS group (three isomers), and TSD group (one isomer). (KIE values for individual TSs are in the Supporting Information.) Among each group, KIE values are averaged on the basis of the Boltzmann weights of each TS, according to corresponding free-energy barriers.

Owing to the fairly lower free-energy barriers of TSP and TSD than those of other TS groups (ETS/TSPR/LTS groups), TSP or TSD has little chance to be the rate-limiting step. Therefore, we turn our attention to ETSs, TSPRs, and LTSs. From Table 3, ETS, TSPR, and LTS groups have

Table 3. Averaged Computed KIE Values for Each TS Group for Acid-Catalyzed Isomerization Reactions[a]

	TSP group	ETS group	TSPR group	LTS group	TSD group
$^{14}k_{C^{2'}}$	0.989	0.989	1.001	0.993	1.005
$^{14}k_{C^{3'}}$	0.997	0.985	0.991	0.981	0.981
$^{14}k_{C^{5'}}$	1.004	1.002	1.005	1.002	1.004
$^{18}k_{O^{2'}}$	1.002	1.007	1.006	1.002	0.997
$^{18}k_{O^{3'}}$	0.991	0.996	1.005	1.001	0.996
$^{18}k_{O^{5'}}$	0.995	1.001	1.006	1.001	0.995
$^{18}k_{O^{1P/2P}}$[a]	0.996	1.054	1.011	1.054	0.996

[a]The arithmetic average values of $^{18}k_{O^{1P}}$ and $^{18}k_{O^{2P}}$, *i.e.*, $^{18}k_{O^{1P/2P}} = (^{18}k_{O^{1P}} + {}^{18}k_{O^{2P}})/2$.

distinguishable averaged KIE values. For example, the TSPR group has near unity KIE values for C$^{2'}$ and C$^{3'}$ (1.001 for $^{14}k_{C^{2'}}$ and 0.991 for $^{14}k_{C^{3'}}$), while the ETS/LTS group has inverse KIE values (0.989 for $^{14}k_{C^{2'}}$ and 0.985 for $^{14}k_{C^{3'}}$ in the ETS group, 0.993 for $^{14}k_{C^{2'}}$ and 0.981 for $^{14}k_{C^{3'}}$ in the LTS group). The TSPR group has a slightly normal KIE value for O$^{1P/2P}$ (1.011), in contrast with large normal KIE values for both ETS and LTS groups (both 1.054). KIE values for other sites are all near unity for ETS, TSPR, and LTS groups.

Due to the difficulty in measuring the intrinsic KIE values for acid-catalyzed isomerization between 3′,5′- and 2′,5′-phosphodiesters, unfortunately, we do not have direct experimental results by now, which will be discussed further in the following section.

3.3. Combination of Cleavage and Isomerization Reactions. In the above sections, we made analyses and discussions on the cleavage and isomerization reactions, separately, based on a joint theoretical and experimental study on kinetic isotope effects. Actually, the two reactions occur simultaneously, which makes experimental measurements of KIE values not trivial. In other words, the measured/observed KIE values listed in Table 2 consist of partial contributions from both reactions. Therefore, more strictly, we should extract the intrinsic KIE values (KIE$_{int}$) from the observed KIE values (KIE$_{obs}$), before comparing with our simulations. Northrop's method provides one possible way to do this.[62]

The reaction mechanisms for both the cleavage and isomerization reactions can be minimized as Scheme 4. R, I,

Scheme 4. A Minimal Mechanism for the 2′-O-Transphosphorylation of the 3′,5′-Phosphodiester and the Isomerization between 3′,5′- and 2′,5′-Phosphodiesters

$$\mathrm{R} \underset{k_2}{\overset{k_1}{\rightleftharpoons}} \mathrm{I} \xrightarrow{k_3} \mathrm{P}$$

and P represent the mixture of 3′,5′- and 2′,5′-phosphodiesters, possible phosphorane isomers that can be formed through pseudorotation and 2′,3′-cyclic monophosphates and alcohol leaving groups, respectively. k_1 and k_2 are the reaction rates for the formation of a phosphorane and the breakdown of a phosphorane to a phosphodiester, and k_3 is for the departure of

https://doi.org/10.1021/acs.jctc.2c01277
J. Chem. Theory Comput. 2023, 19, 1322−1332

the leaving groups resulting in products. The primary KIE_{obs} will be affected by commitments as the following relationship[37]

$$KIE_{obs} = \frac{KIE_{int} + C_f + C_r \cdot EIE}{1 + C_f + C_r} \quad (7)$$

where C_f and C_r are defined as the forward and reverse commitments, and EIE is the equilibrium isotope effects, respectively. The forward commitment C_f is defined as the ratio of the isotopically sensitive rate constant in the forward direction to the rate constant for the breakdown of the phosphorane back to 3′,5′- or 2′,5′-phosphodiester. And the reverse commitment C_r is defined as the ratio of the isotopically sensitive rate constant in the reverse direction to the rate constant for the cleavage of the phosphorane to products. Particularly, in the case of an irreversible isotopically sensitive process, C_r goes to zero, and the above equation can be simplified as follows:

$$KIE_{obs} = \frac{KIE_{int} + C_f}{1 + C_f} \quad (8)$$

There are several experimental methods to obtain C_f and C_r or eliminate them. For simplicity, here we just assume reasonable values for C_f and C_r to evaluate the intrinsic KIE values.

Taking the KIE value for the leaving group ($^{18}k_{O^{5'}}$) for example, since k_3 is the only isotope-sensitive step, so C_r equals zero, and C_f can be written as

$$C_f = \frac{k_3}{k_2} \quad (9)$$

As proposed in Schemes 2, 3, and S8, a phosphorane may break down in one pathway to cleave to 2′,3′-cyclic monophosphate and the leaving group or in six pathways to reform the 3′,5′- or 2′,5′-phosphodiester. Thus, C_f would be small and consequently hardly affects the observed KIE value. For example, if we simply assume the reaction rates for these pathways are equal, the forward commitment would be $1/7 \approx 0.14$. Then the extracted intrinsic $^{18}k_{O^{5'}}$ value is 1.006, which is almost unchanged from the observed KIE value of 1.005 (Table 2).

For secondary KIE values, since both the formation (k_1) and the breakdown (k_2 and k_3) of the phosphorane are isotopically sensitive steps, thus the observed KIE can be described as follows:

$$KIE_{obs} = KIE_{int,1} \cdot \frac{KIE_{int,3}/KIE_{int,2} + C_f}{1 + C_f} \quad (10)$$

Similarly, if we simply assume that $KIE_{int,2}$ and $KIE_{int,3}$ are the same, then the above equation can be simplified as

$$KIE_{obs} = KIE_{int,1} \quad (11)$$

Based on the above analyses, the commitments would have little influence on the observed KIE values for the cleavage reaction, and the experimental results in Table 2 are reliable.

Finally, we can combine our investigations on acid-catalyzed cleavage of 3′,5′-phosphodiester by 2′-O-transphosphorylation with isomerization between 3′,5′- and 2′,5′-phosphodiesters, through the pH-rate profiles shown in Figure 1.

Under strong acidic conditions (pH < 2), the two pH-rate profiles are quite close to each other, and the reaction rate of isomerization is always slightly slower than that of the 2′-O-transphosphorylation process. By using eq 1, reading the reaction rate constants for the two profiles at pH = 0, we can evaluate the corresponding free-energy barriers are 24.2 and 24.0 kcal mol^{-1} for the cleavage and isomerization reactions, respectively. In our simulations, for the acid-catalyzed cleavage reaction, the ETS is the rate-limiting transition state, and the free-energy barrier is 18.0 kcal mol^{-1}. While for the acid-catalyzed isomerization reaction, the result shows that pseudorotation is the rate-limiting step, and the free-energy barrier is in the range of 19.4−21.1 kcal mol^{-1} (six isomers of TSPRs). These results are well consistent with the experimental observation. It also means that though the two reactions have similar pH-rate dependence, the rate-limiting steps are quite different.

The underestimated theoretical free-energy barriers than experimental measurements may result from that, in our simulation, we calculate the case for extremely acidic conditions. While in experiments, the measurements may mix with contributions from other optional pathways with higher activation energies. For example, in the rate-limiting step ETS for the acid-catalyzed cleavage reaction, the nucleophilic attack occurs with both O^{1P} and O^{2P} protonated. Considering the pK_a value of the starting material (pK_a < 0.7 between monocationic and neutral RSs) and real acidity in experiment, this process may also occur with only one of O^{1P}/O^{2P} protonated, which has a higher free-energy barrier (∼30.0 kcal mol^{-1}). The experimental measurement may be the mixture of the two partial contributions. However, for the acid-catalyzed isomerization reaction, the calculated free-energy barriers of the rate-limiting TSPRs are very close to the experimental results. This is because the pK_a value for the neutral phosphorane structure with both O^{1P} and O^{2P} protonated to the anionic structure after dissociating one proton from O^{1P}/O^{2P} is fairly large (∼11), thus most of the phosphoranes will remain neutral in strong acidic conditions, though TSPRs with only one of O^{1P}/O^{2P} protonated have even lower free-energy barriers than that of neutral ones.

When 2 < pH < 8, the reaction rate for the cleavage reaction first slows down (2 < pH < 5) and then speeds up (5 < pH < 8), while the reaction rate for the isomerization reaction is nearly pH-independent in this region. For the cleavage reaction, both ETS and LTS contain proton transfer processes, thus these two TSs are both dependent on the concentration of H_3O^+ ions. With pH increases, the rate-limiting step may transfer from the nucleophilic attack occurring with both O^{1P} and O^{2P} protonated, to a neutral ETS/LTS with only one of the O^{1P}/O^{2P} protonated (free-energy barriers ∼30.0 kcal mol^{-1}), to an anionic ETS/LTS with both O^{1P} and O^{2P} unprotonated (free-energy barriers ∼40.0 kcal mol^{-1}), to a dianionic ETS/LTS (the ETS and LTS in the base-catalyzed cleavage reaction, free-energy barriers ∼21.0 kcal mol^{-1}). This is the origin of the reaction rate first slowing down and then speeding up in this pH range. For the isomerization reaction, situations are more complicated. On the one hand, with an increase in the pH, the dissociation of the cationic intermediate may lead to the increase in the free-energy barrier of the nucleophilic attack of $O^{2'}$ or departure of $O^{3'}$ (as we discussed above on a neutral ETS/LTS for the cleavage reaction in this pH range). On the other hand, the dissociation of the phosphorane will lower the free-energy barrier of pseudorotation (Free-energy barrier of the TSPR with only one of O^{1P}/O^{2P} protonated is ∼3.0 kcal mol^{-1} lower than that of both O^{1P} and O^{2P} protonated.). The competition in between results in a pH-independent-like curve in Figure 1. In other words, in

https://doi.org/10.1021/acs.jctc.2c01277
J. Chem. Theory Comput. 2023, 19, 1322−1332

this pH range, the rate-limiting step transfers from pseudorotation to the nucleophilic attack or departure of $O^{3'}$, gradually.

When pH > 8, for the cleavage reaction, the dianionic ETS and LTS gradually dominate in the reaction, and thus the reaction rate speeds up. (In previous work on the base-catalyzed cleavage reaction, the LTS is the rate-limiting step and has a free-energy barrier of ∼21.0 kcal mol^{-1}.) While for the isomerization reaction, although the shared ETS and LTS with the base-catalyzed cleavage reaction can participate with fair low free-energy barriers, the dianionic phosphorane is too short-lived to undergo other processes, e.g. pseudorotation. Therefore, no isomerization is observed in this pH range.

To sum up, all the above simulations are fairly consistent with current experimental results. However, we are still looking forward to further experimental data for both acid-catalyzed RNA cleavage and isomerization reactions to give the final conclusion.

4. CONCLUSION

In summary, we proposed several reaction schemes for modeling different mechanisms of RNA cleavage by 2′-O-transphosphorylation of 3′,5′-phosphodiester and isomerization between 3′,5′- and 2′,5′-phosphodiesters in the acidic solution. Reaction pathways in Schemes 2 and 3, which involve sufficient explicit H_2O molecule(s) and H_3O^+ ion(s), are the most promising candidates for the two reactions, respectively.

For the acid-catalyzed cleavage reaction, the reaction pathway reveals a very different reaction mechanism compared with conclusions on base- and RNase-A-catalyzed reactions. For example, both nonbridging oxygens O^{1P} and O^{2P} need to be protonated in order for considerably lowering free-energy barriers. In addition to free-energy barriers, the $ETS^{\{1\}}$ and $LTS^{\{1a\}}$ both have KIE values consistent with experimental data. Especially, the inverse KIE value for the nucleophile of the $ETS^{\{1\}}$ gives us a new horizon regarding possible nucleophilic KIE values of ETSs when the deprotonation of $O^{2'}$−H is not a pre-equilibrium step. Furthermore, the $IS^{\{1b\}}$-$LTS^{\{1\}}$ energy plateau is a trait exclusively for the acid-catalyzed cleavage reaction, which is absent from the base-catalyzed case. This iconic plateau at low pH, in which the system can freely roam around, should provide much more chances for the collapse of the phosphorane intermediate through a pseudorotation to produce the 2′,5′-phosphodiester isomer.

For the acid-catalyzed isomerization reaction between 3′,5′- and 2′,5′-phosphodiesters, though it shares a common nucleophilic attack process (ETS) with the acid-catalyzed cleavage reaction, the rate-limiting steps are different for the two reactions. In the cleavage reaction, the shared ETS is the rate-limiting step; while for the isomerization reaction, the rate-limiting step is the pseudorotation. KIE values are also provided. Though at present we do not have experimental measurements for such KIE values to verify the conclusion, it provides a good direction to support our results.

At last, our investigations on acid-catalyzed cleavage and isomerization reactions are combined through the pH-rate profiles for the two reactions, which also shed light on reaction mechanism(s) near neutral pH conditions. Considering the forward and reverse commitments between the two reactions, all current results are consistent with the experimental data.

ASSOCIATED CONTENT

Supporting Information

The Supporting Information is available free of charge at https://pubs.acs.org/doi/10.1021/acs.jctc.2c01277.

Computational section, determination of reactant state, acid-catalyzed cleavage reaction, acid-catalyzed isomerization reaction, Cartesian coordinates, and references (PDF)

AUTHOR INFORMATION

Corresponding Authors

Yuqing Xu − *School of Physics and Optoelectronic Engineering, Ludong University, Yantai 264025, China;* orcid.org/0000-0001-8864-3112; Email: physxyq@ldu.edu.cn

Darrin M. York − *Department of Chemistry and Chemical Biology, Rutgers, The State University of New Jersey, Piscataway, New Jersey 08854, United States;* orcid.org/0000-0002-9193-7055; Email: darrin.york@rutgers.edu

Kin-Yiu Wong − *Department of Physics, High Performance Cluster Computing Centre, Institute of Advanced Materials, Institute of Computational and Theoretical Studies, Hong Kong Baptist University, Kowloon Tong, Hong Kong; Institute of Research and Continuing Education, Hong Kong Baptist University (Shenzhen), Shenzhen 518057, China;* Present Address: PO Box 68233, Kowloon East Post Office, Hong Kong; Email: kywong.researcher@gmail.com, kiniu@alumni.cuhk.net

Author

Michael E. Harris − *Department of Chemistry, University of Florida, Gainesville, Florida 32611, United States;* orcid.org/0000-0001-8977-4392

Complete contact information is available at: https://pubs.acs.org/10.1021/acs.jctc.2c01277

Notes

The authors declare no competing financial interest.

ACKNOWLEDGMENTS

Computing resources were provided by Inspur TS10K High Performance Computing Cluster at Ludong University. The authors are grateful for financial support provided by the National Institutes of Health (GM62248 to D.M.Y. and GM127100 to M.E.H.).

REFERENCES

(1) Chung, C. W.; Mahler, H. R. Incorporation of adenine nucleotide into internucleotide linkages of RNA. *Biochem. Biophys. Res. Commun.* **1959**, *1*, 232−235.

(2) Westheimer, F. H. Why nature chose phosphates. *Science* **1987**, *235*, 1173−1178.

(3) Steitz, T. A.; Steitz, J. A. A general two-metal-ion mechanism for catalytic RNA. *Proc. Natl. Acad. Sci. U. S. A.* **1993**, *90*, 6498−6502.

(4) Perreault, D. M.; Anslyn, E. V. Unifying the current data on the mechanism of cleavage−transesterification of RNA. *Angew. Chem., Int. Ed.* **1997**, *36*, 432−450.

(5) Oivanen, M.; Kuusela, S.; Lönnberg, H. Kinetics and mechanisms for the cleavage and isomerization of the phosphodiester bonds of RNA by Brønsted acids and bases. *Chem. Rev.* **1998**, *98*, 961−990.

(6) Raines, R. T. Ribonuclease A. *Chem. Rev.* **1998**, *98*, 1045−1066.

(7) Strobel, S. A.; Cochrane, J. C. RNA catalysis: Ribozymes, ribosomes, and riboswitches. *Curr. Opin. Chem. Biol.* **2007**, *11*, 636−643.
(8) Lassila, J. K.; Zalatan, J. G.; Herschlag, D. Biological phosphoryl-transfer reactions: Understanding mechanism and catalysis. *Annu. Rev. Biochem.* **2011**, *80*, 669−702.
(9) Soukup, G. A. In *Catalytic RNA*; Soukup, G. A., Ed.; Progress in molecular biology and translational science; Academic Press: San Diego, USA, 2013; Vol. *120*, p xi, DOI: 10.1016/B978-0-12-381286-5.09987-X.
(10) Jarvinen, P.; Oivanen, M.; Lönnberg, H. Interconversion and phosphoester hydrolysis of 2′, 5′-dinucleoside and 3′, 5′-dinucleoside monophosphates - kinetics and mechanisms. *J. Org. Chem.* **1991**, *56*, 5396−5401.
(11) Gerratana, B.; Sowa, G. A.; Cleland, W. W. Characterization of the transition-state structures and mechanisms for the isomerization and cleavage reactions of uridine 3′-m-nitrobenzyl phosphate. *J. Am. Chem. Soc.* **2000**, *122*, 12615−12621.
(12) Gu, H.; Zhang, S. M.; Wong, K. Y.; Radak, B. K.; Dissanayake, T.; Kellerman, D. L.; Dai, Q.; Miyagi, M.; Anderson, V. E.; York, D. M.; Piccirilli, J. A.; Harris, M. E. Experimental and computational analysis of the transition state for ribonuclease A-catalyzed RNA 2′-O-transphosphorylation. *Proc. Natl. Acad. Sci. U. S. A.* **2013**, *110*, 13002−13007.
(13) Harris, M. E.; Piccirilli, J. A.; York, D. M. Integration of kinetic isotope effect analyses to elucidate ribonuclease mechanism. *Biochim. Biophys. Acta - Proteins Proteom.* **2015**, *1854*, 1801−1808.
(14) Zhang, S. M.; Gu, H.; Chen, H. Y.; Strong, E.; Ollie, E. W.; Kellerman, D.; Liang, D.; Miyagi, M.; Anderson, V. E.; Piccirilli, J. A.; York, D. M.; Harris, M. E. Isotope effect analyses provide evidence for an altered transition state for RNA 2′-O-transphosphorylation catalyzed by Zn^{2+}. *Chem. Commun.* **2016**, *52*, 4462−4465.
(15) Wong, K. Y.; Gu, H.; Zhang, S. M.; Piccirilli, J. A.; Harris, M. E.; York, D. M. Characterization of the reaction path and transition states for RNA transphosphorylation models from theory and experiment. *Angew. Chem., Int. Ed.* **2012**, *51*, 647−651.
(16) Wong, K. Y.; Xu, Y.; York, D. M. Ab initio path-integral calculations of kinetic and equilibrium isotope effects on base-catalyzed RNA transphosphorylation models. *J. Comput. Chem.* **2014**, *35*, 1302−1316.
(17) Wong, K. Y.; Xu, Y.; Xu, L. Review of computer simulations of isotope effects on biochemical reactions: From the Bigeleisen equation to Feynman's path integral. *Biochim. Biophys. Acta - Proteins Proteom.* **2015**, *1854*, 1782−1794.
(18) Tiesinga, E.; Mohr, P. J.; Newell, D. B.; Taylor, B. N. Values of fundamental physical constants. Available from: http://physics.nist.gov/cuu/Constants/ (accessed 2023-02-02).
(19) Wong, K. Y.; Richard, J. P.; Gao, J. L. Theoretical analysis of kinetic isotope effects on proton transfer reactions between substituted α-methoxystyrenes and substituted acetic acids. *J. Am. Chem. Soc.* **2009**, *131*, 13963−13971.
(20) Chen, H. Y.; Giese, T. J.; Huang, M.; Wong, K. Y.; Harris, M. E.; York, D. M. Mechanistic insights into RNA transphosphorylation from kinetic isotope effects and linear free energy relationships of model reactions. *Chem. -Eur. J.* **2014**, *20*, 14336−14343.
(21) Lee, T. S.; Radak, B. K.; Huang, M.; Wong, K. Y.; York, D. M. Roadmaps through free energy landscapes calculated using the multidimensional vFEP approach. *J. Chem. Theory Comput.* **2014**, *10*, 24−34.
(22) Parr, R. G.; Yang, W. *Density-Functional Theory of Atoms and Molecules*; Oxford University Press: New York, 1989.
(23) Kohn, W. Nobel Lecture: Electronic structure of matter-wave functions and density functionals. *Rev. Mod. Phys.* **1999**, *71*, 1253−1266.
(24) York, D. M.; Karplus, M. A smooth solvation potential based on the conductor-like screening model. *J. Phys. Chem. A* **1999**, *103*, 11060−11079.
(25) Cossi, M.; Scalmani, G.; Rega, N.; Barone, V. New developments in the polarizable continuum model for quantum mechanical and classical calculations on molecules in solution. *J. Chem. Phys.* **2002**, *117*, 43−54.
(26) Khandogin, J.; Gregersen, B. A.; Thiel, W.; York, D. M. Smooth solvation method for d-orbital semiempirical calculations of biological reactions. 1. Implementation. *J. Phys. Chem. B* **2005**, *109*, 9799−9809.
(27) Frisch, M. J.; Trucks, G. W.; Schlegel, H. B.; Scuseria, G. E.; Robb, M. A.; Cheeseman, J. R.; Scalmani, G.; Barone, V.; Mennucci, B.; Petersson, G. A.; Nakatsuji, H.; Caricato, M.; Li, X.; Hratchian, H. P.; Izmaylov, A. F.; Bloino, J.; Zheng, G.; Sonnenberg, J. L.; Hada, M.; Ehara, M.; Toyota, K.; Fukuda, R.; Hasegawa, J.; Ishida, M.; Nakajima, T.; Honda, Y.; Kitao, O.; Nakai, H.; Vreven, T.; Montgomery, J. A., Jr.; J, E. P.; Ogliaro, F.; Bearpark, M.; Heyd, J. J.; Brothers, E.; Kudin, K. N.; Staroverov, V. N.; Keith, T.; Kobayashi, R.; Normand, J.; Raghavachari, K.; Rendell, A.; Burant, J. C.; Iyengar, S. S.; Tomasi, J.; Cossi, M.; Rega, N.; Millam, J. M.; Klene, M.; Knox, J. E.; Cross, J. B.; Bakken, V.; Adamo, C.; Jaramillo, J.; Gomperts, R.; Stratmann, R. E.; Yazyev, O.; Austin, A. J.; Cammi, R.; Pomelli, C.; Ochterski, J. W.; Martin, R. L.; Morokuma, K.; Zakrzewski, V. G.; Voth, G. A.; Salvador, P.; Dannenberg, J. J.; Dapprich, S.; Daniels, A. D.; Farkas, O.; Foresman, J. B.; Ortiz, J. V.; Cioslowski, J.; Fox, D. J. *Gaussian 09*, Revision C.01; 2009.
(28) Scalmani, G.; Frisch, M. J. Continuous surface charge polarizable continuum models of solvation. I. General formalism. *J. Chem. Phys.* **2010**, *132*, 114110.
(29) McQuarrie, D. A. *Statistical Mechanics*, illustrated ed.; University Science Books: New York, USA, 2000; p 641.
(30) Schramm, V. L. Enzymatic transition states and transition state analog design. *Annu. Rev. Biochem.* **1998**, *67*, 693−720.
(31) Hengge, A. C. Isotope effects in the study of phosphoryl and sulfuryl transfer reactions. *Acc. Chem. Res.* **2002**, *35*, 105−112.
(32) Cleland, W. W. The use of isotope effects to determine enzyme mechanisms. *Arch. Biochem. Biophys.* **2005**, *433*, 2−12.
(33) Liu, Y.; Gregersen, B. A.; Hengge, A.; York, D. M. Transesterification thio effects of phosphate diesters: Free energy barriers and kinetic and equilibrium isotope effects from density-functional theory. *Biochemistry* **2006**, *45*, 10043−10053.
(34) Schramm, V. L. Introduction: Principles of enzymatic catalysis. *Chem. Rev.* **2006**, *106*, 3029−3030.
(35) Strassner, T. Isotope effects in chemistry and biology. *Angew. Chem., Int. Ed.* **2006**, *45*, 6420−6421.
(36) Cassano, A. G.; Wang, B.; Anderson, D. R.; Previs, S.; Harris, M. E.; Anderson, V. E. Inaccuracies in selected ion monitoring determination of isotope ratios obviated by profile acquisition: Nucleotide $^{18}O/^{16}O$ measurements. *Anal. Biochem.* **2007**, *367*, 28−39.
(37) Cook, P. F.; Cleland, W. W. *Enzyme Kinetics and Mechanism*; Taylor & Francis Group: New York, Oxon, 2007; DOI: 10.4324/9780203833575.
(38) Bigeleisen, J. The relative reaction velocities of isotopic molecules. *J. Chem. Phys.* **1949**, *17*, 675−678.
(39) Bigeleisen, J. Chemistry of isotopes. *Science* **1965**, *147*, 463.
(40) Bigeleisen, J.; Lee, M. W.; Mandel, F. Equilibrium isotope effects. *Annu. Rev. Phys. Chem.* **1973**, *24*, 407−440.
(41) Pupyshev, V. I.; Panchenko, Y. N.; Stepanov, N. F. A new derivation for the Teller-Redlich isotopic product rule. *Vib. Spectrosc.* **1994**, *7*, 191−196.
(42) Schaad, L. J.; Bytautas, L.; Houk, K. N. Ab initio test of the usefulness of the Redlich-Teller product rule in computing kinetic isotope effects. *Can. J. Chem.* **1999**, *77*, 875−878.
(43) Anisimov, V.; Paneth, P. ISOEFF98. A program for studies of isotope effects using Hessian modifications. *J. Math. Chem.* **1999**, *26*, 75−86.
(44) Wolfsberg, M. *Isotope Effects in Chemistry and Biology*; Taylor & Francis Group: Boca Raton, 2006; Chapter 3, p 89, DOI: 10.1201/9781420028027.ch3.
(45) Feynman, R. P.; Hibbs, A. R.; Styer, D. F. *Quantum Mechanics and Path Integrals*, emended ed.; Dover Publications: Mineola, NY, 2005.

(46) Kleinert, H. *Path Integrals in Quantum Mechanics, Statistics, Polymer Physics, and Financial Markets*, 5th ed.; World Scientific Singapore: Hackensack, NJ, 2009; DOI: 10.1142/7305.
(47) Wong, K. Y. Review of Feynman's path integral in quantum statistics: From the molecular Schrodinger equation to Kleinert's variational perturbation theory. *Commun. Comput. Phys.* **2014**, *15*, 853−894.
(48) Wong, K. Y.; Gao, J. An automated integration-free path-integral method based on Kleinert's variational perturbation theory. *J. Chem. Phys.* **2007**, *127*, 211103.
(49) Wong, K. Y.; Gao, J. Systematic approach for computing zero-point energy, quantum partition function, and tunneling effect based on Kleinert's variational perturbation. *J. Chem. Theory Comput.* **2008**, *4*, 1409−1422.
(50) *MATHEMATICA*, Version 6.0; Wolfram Research, Inc.: 2007.
(51) Wong, K. Y.; Gao, J. The reaction mechanism of paraoxon hydrolysis by phosphotriesterase from combined QM/MM simulations. *Biochemistry* **2007**, *46*, 13352−13369.
(52) López, C. S.; Faza, O. N.; de Lera, A. R.; York, D. M. Pseudorotation barriers of biological oxyphosphoranes: A challenge for simulations of ribozyme catalysis. *Chem. -Eur. J.* **2005**, *11*, 2081−2093.
(53) Lopez, X.; Dejaegere, A.; Leclerc, F.; York, D. M.; Karplus, M. Nucleophilic attack on phosphate diesters: A density functional study of in-line reactivity in dianionic, monoanionic, and neutral systems. *J. Phys. Chem. B* **2006**, *110*, 11525−11539.
(54) Linjalahti, H.; Feng, G.; Mareque-Rivas, J. C.; Mikkola, S.; Williams, N. H. Cleavage and isomerization of UpU promoted by dinuclear metal ion complexes. *J. Am. Chem. Soc.* **2008**, *130*, 4232−4233.
(55) Lain, L.; Lönnberg, H.; Lönnberg, T. Intramolecular participation of amino groups in the cleavage and isomerization of ribonucleoside 3′-phosphodiesters: The role in stabilization of the phosphorane intermediate. *Chem. -Eur. J.* **2013**, *19*, 12424−12434.
(56) Harris, M. E.; Dai, Q.; Gu, H.; Kellerman, D. L.; Piccirilli, J. A.; Anderson, V. E. Kinetic isotope effects for RNA cleavage by 2′-O-transphosphorylation: Nucleophilic activation by specific base. *J. Am. Chem. Soc.* **2010**, *132*, 11613−11621.
(57) Anslyn, E.; Breslow, R. On the mechanism of catalysis by ribonuclease: Cleavage and isomerization of the dinucleotide UpU catalyzed by imidazole buffers. *J. Am. Chem. Soc.* **1989**, *111*, 4473−4482.
(58) Oivanen, M.; Schnell, R.; Pfleiderer, W.; Lönnberg, H. Interconversion and hydrolysis of monomethyl and monoisopropyl esters of adenosine 2′- and 3′-monophosphates: Kinetics and mechanisms. *J. Org. Chem.* **1991**, *56*, 3623−3628.
(59) Kuusela, S.; Lönnberg, H. Hydrolysis and isomerization of the internucleosidic phosphodiester bonds of polyuridylic acid: Kinetics and mechanism. *J. Chem. Soc., Perkin Trans.* **1994**, *2*, 2109−2113.
(60) Kluger, R.; Covitz, F.; Dennis, E.; Williams, L. D.; Westheimer, F. H. pH-product and pH-rate profiles for the hydrolysis of methyl ethylene phosphate. Rate-limiting pseudorotation. *J. Am. Chem. Soc.* **1969**, *91*, 6066−6072.
(61) Lopez, X.; Schaefer, M.; Dejaegere, A.; Karplus, M. Theoretical evaluation of pK_a in phosphoranes: Implications for phosphate ester hydrolysis. *J. Am. Chem. Soc.* **2002**, *124*, 5010−5018.
(62) Northrop, D. B. *Enzyme Mechanism from Isotope Effects*; CRC Press: Boca Raton, 1991; Chapter 6, p 181.

https://doi.org/10.1021/acs.jctc.2c01277
J. Chem. Theory Comput. 2023, 19, 1322−1332